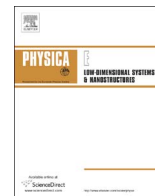




ELSEVIER

Contents lists available at ScienceDirect

Physica E

journal homepage: [www.elsevier.com/locate/physce](http://www.elsevier.com/locate/physce)

# Optimal control of a charge qubit in a double quantum dot with a Coulomb impurity



Diego S. Acosta Coden, Rodolfo H. Romero, Alejandro Ferrón\*, Sergio S. Gomez

*Instituto de Modelado e Innovación Tecnológica (CONICET-UNNE) and Facultad de Ciencias Exactas y Naturales y Agrimensura, Universidad Nacional del Nordeste, Avenida Libertad 5400, W3404AAS Corrientes, Argentina*

## A B S T R A C T

We study the efficiency of modulated external electric pulses to produce efficient and fast charge localization transitions in a two-electron double quantum dot. We use a configuration interaction method to calculate the electronic structure of a quantum dot model within the effective mass approximation. The interaction with the electric field is considered within the dipole approximation and optimal control theory is applied to design high-fidelity ultrafast pulses in pristine samples. We assessed the influence of the presence of Coulomb charged impurities on the efficiency and speed of the pulses. A protocol based on a two-step optimization is proposed for preserving both advantages of the original pulse. The processes affecting the charge localization is explained from the dipole transitions of the lowest lying two-electron states, as described by a discrete model with an effective electron-electron interaction.

## 1. Introduction

Semiconductor quantum dots (QDs) are excellent candidates for realizing qubits for quantum information processing because of the manipulability, scalability and tunability of their electronic and optical properties [1–4]. Advances in semiconductor technology allow the preparation of complex structures and a fine experimental control of the parameters defining their electrical and optical properties [5–7].

In recent years there has been an increasing interest in controlling quantum phenomena in molecular systems and nanodevices [8–15], due to the possibility to modify the wave function of the system through the appropriate tailoring of external fields. Coherent quantum control of electrons in quantum dots exposed to electromagnetic radiation is of great interest in many technological applications from charge transport devices to quantum information [16–18]. Several studies in quantum control of double quantum dots (DQDs) has been performed using gate voltages and optimized laser pulses [19–21]. In addition, the number of quantum control experiments is rapidly rising through the improvement of laser pulse shaping and closed-loop learning techniques [19–21].

Among other techniques, Optimal Control Theory (OCT) [22–25] has become an efficient tool for designing external fields able to control quantum processes. The optimal field is the field employed in order to steer a dynamical system from a initial state to a desired target state minimizing a cost functional which generally penalizes the energy (fluence) of the pulse. A great effort has been invested in recent years in

the development of different methods in order to solve the optimal equations [26–30]. Monotonically convergent iterative schemes proposed by Tannor et al. [31] and Rabitz et al. [32] have been successfully applied to the control of different quantum phenomena, mainly related to chemical process [33,34]. In the last years, optimal control theory became a research area that has received increasing interest from the scientists studying emerging fields within quantum information science [35,36]. Modern quantum devices are systems where the wave function must be manipulated with highest possible precision using, for example, quantum gates. This high-fidelity quantum engineering needs new and efficient strategies which allow an optimal suppression of environment losses during gating or optical control. In addition, quantum computation theoretically requires extremely high fidelity in the elementary quantum state transformations. Optical control of quantum dot based devices is of fundamental interest for a wide range of applications in quantum information [35–40]. For example, optical manipulation is an alternative in order to store qubits in the electron spin [35]. Hansen et al. [36] show that carefully selected microwave pulses can be used to populate a single state of the first excitation band in a two-electron DQD and that the transition time can be decreased using optimal pulse control. Heller et al. [41] show that the quality of periodic recurrence (quantum revival) in the time evolution in a quantum well, can be restored almost completely by coupling the system to an electromagnetic field obtained using quantum optimal control theory. It results clear that the study of quantum dynamics of nanodevices and the possibility of controlling different processes in

\* Corresponding author.

such systems represent an important research field with very interesting technological applications. The implementation of numerical techniques such as OCT allow us to analyze different possibilities and scenarios in order to construct and improve nanodevices based quantum bits.

It is known that the presence of impurity centers has a great influence on the optical and electronic properties of nanostructured materials. Recent works [42–48] studied the effects of having unintentional charged impurities in two-electron laterally coupled two-dimensional double quantum-dot systems. They analyzed the effects of quenched random-charged impurities on the singlet-triplet exchange coupling and spatial entanglement in two-electron double quantum-dots. Although there is an enormous interest in applying these systems in quantum information technologies, there are few works trying to quantify the effect of charged impurities on this kind of tasks. The existence of unintentional impurities, which are always present in nanostructured devices, affects seriously the possibility of using these devices as quantum bits. Although the distribution and concentration of impurities in these systems result unknown parameters, there are some recent works that propose the possibility of experimentally control these issues [49–52]. Impurity doping in semiconductor materials is considered as a useful technology that has been exploited to control optical and electronic properties in different nanodevices.

It is worth to mention that, due to environmental perturbations, these systems lose coherence. For example, confined electrons interact with spin nuclei through the hyperfine interaction leading, inevitably, to decoherence [3]. Even, having just one charged impurity could induce qubit decoherence if this impurity is dynamic and has a fluctuation time scale comparable to gate operation time scales [42]. Decoherence is a phenomenon that plays a central role in quantum information and its technological applications [53–62]. The short transition time in optically driven processes reduces the effect of decoherence sources, such as hyperfine or phonon interactions. A number of known quantum control techniques such as quantum bang-bang control [63] or spin-echo pulses [3] allow experimentalists to fight decoherence. It seems reasonable that optimal control theory can be considered as a tool in order to design control pulses or gates so that quantum systems can be controlled in presence of environmental couplings without suffering significant decoherence.

The aim of this work is to present a detailed analysis of the optical control of two electrons in a two-dimensional coupled quantum dot and the effect of impurities by means of Optimal Control Theory. The paper is organized as follows. In Section 2 we introduce the model for the two-dimensional two-electron coupled quantum dot and briefly describe the method used to calculate its electronic structure. In Section 2.2, we describe optimal control equations for a two-dimensional two-electron coupled quantum dot. In Section 3 we analyze the operation of a charge qubit in presence of impurities. In Section 4, we propose a protocol of initialization (Section 4.1) and operation (Section 4.2) of the qubit using electromagnetic pulses avoiding the effects of the impurities by means of OCT. Finally, in Section 5 we summarize the conclusions with a discussion of the most relevant points of our analysis.

## 2. Model and calculation method

We consider two laterally coupled two-dimensional quantum dots whose centers are separated a distance  $d$  from each other, and containing two electrons. In quantum dots electrostatically produced, both their size and separation can be controlled by variable gate voltages through metallic electrodes deposited on the heterostructure interface. The eventual existence of doping hydrogenic impurities, probably arising from Si dopant atoms in the GaAs quantum well, have been experimentally studied [45]. These impurities have been theoretically analyzed with a superimposed attractive  $1/r$ -type potential [46,47]. Furthermore, some avoided crossing and lifted degeneracies in

the spectra of single-electron transport experiments have been attributed to negatively charged Coulomb impurities located near to the QD [48]. From fitting the experimental transport spectra to a single-electron model of softened parabolic confinement with a Coulomb charge  $q$ , a set of parameters are obtained; among them, a radius of confinement of 15.5 nm, a confinement frequency  $\hbar\omega = 13.8$  meV and an impurity charge of approximately 1 or 2 electron charges. Indeed, the uncertainty in the parameters and the suppositions introduced in the model does not allow one to precisely ensure the impurity charge, with the screening probably reducing its effective value to less than an electron charge. Therefore, we consider the charge of the doping atom  $Ze$  as a parameter varying in the range  $0 \leq Z \leq 1$ , in order to explore its effect on the properties of the system.

### 2.1. Electronic structure and dynamics

In this work we model the Hamiltonian of the two-dimensional two-electron coupled quantum dot in presence of charged impurities within the single conduction-band effective-mass approximation [37], namely,

$$H_0 = h(\mathbf{r}_1) + h(\mathbf{r}_2) + \frac{e^2}{4\pi\epsilon\epsilon_0 r_{12}}, \quad (1)$$

where  $\mathbf{r}_i = (x_i, y_i)$  ( $i=1,2$ ) and

$$h(\mathbf{r}) = -\frac{\hbar^2}{2m^*} \nabla^2 + V_L(\mathbf{r}) + V_R(\mathbf{r}) + V_A(\mathbf{r}), \quad (2)$$

where  $h(\mathbf{r})$  is the single-electron Hamiltonian that includes the kinetic energy of the electrons, in terms of their effective mass  $m^*$ , and the confining potential for the left and right quantum dots  $V_L$  and  $V_R$ , and the interaction of the electrons with the charged impurities,  $V_A$ .

The last term of the Hamiltonian, Eq. (1), represents the Coulomb repulsive interaction between both electrons at a distance  $r_{12} = |\mathbf{r}_2 - \mathbf{r}_1|$  apart from each other, within a material of effective dielectric constant  $\epsilon$ . We model the confinement with Gaussian attractive potentials

$$V_i(\mathbf{r}) = -V_0 \exp\left(-\frac{1}{2a^2} |\mathbf{r} - \mathbf{R}_i|^2\right), \quad (i = L, R), \quad (3)$$

where  $\mathbf{R}_L$  and  $\mathbf{R}_R$  are the positions of the center of the left and right dots,  $V_0$  denotes the depth of the potential and  $a$  can be taken as a measure of its range. Along this work, we will consider a single impurity atom centered at  $\mathbf{R}_A$ , and modelled as a hydrogenic two-dimensional Coulomb potential

$$V_A(\mathbf{r}) = -\frac{Ze^2}{4\pi\epsilon\epsilon_0 |\mathbf{R}_A - \mathbf{r}|} \quad (4)$$

Since the Hamiltonian does not depend on the electron spin, its eigenstates can be factored out as a product of a spatial and a spin part

$$\Psi_i(\mathbf{r}_1, \mathbf{r}_2, m_{s_1}, m_{s_2}) = \Psi_i^S(\mathbf{r}_1, \mathbf{r}_2) \chi_{S,M}, \quad (5)$$

where  $S=0, 1$  for singlet and triplet states, respectively, and  $M = m_{s_1} + m_{s_2}$  is the total spin projection.

The eigenstates of the model Hamiltonian can be obtained by direct diagonalization in a finite basis set [64]. The spatial part is obtained, in a full configuration interaction (CI) calculation, as

$$\Psi_m^S(\mathbf{r}_1, \mathbf{r}_2) = \sum_{n=1}^{N_{\text{conf}}} c_{mn}^S \Phi_n^S(\mathbf{r}_1, \mathbf{r}_2) \quad (6)$$

where  $N_{\text{conf}}$  is the number of singlet ( $S=0$ ) or triplet ( $S=1$ ) two-electron configurations  $\Phi_n^S(\mathbf{r}_1, \mathbf{r}_2)$  considered, and  $n = (i, j)$  is a configuration label obtained from the indices  $i$  and  $j$  from a single electron basis, i.e.,

$$\Phi_n^S(\mathbf{r}_1, \mathbf{r}_2) = \frac{1}{\sqrt{2}} [\phi_i(\mathbf{r}_1) \phi_j(\mathbf{r}_2) + (1 - 2S) \phi_j(\mathbf{r}_1) \phi_i(\mathbf{r}_2)] \quad (7)$$

for  $i \neq j$ , and  $\Phi_n^{S=0}(\mathbf{r}_1, \mathbf{r}_2) = \phi_i(\mathbf{r}_1) \phi_i(\mathbf{r}_2)$  for the doubly occupied singlet

states.

We chose a single-particle basis of Gaussian functions, centered at the dots and atom positions  $\mathbf{R}_p$  ( $P = L, R, A$ ), of the type [65,66]

$$\phi_i(\mathbf{r}) = N(x - P_x)^{m_i}(y - P_y)^{n_i} \exp(-\alpha_i |\mathbf{r} - \mathbf{R}_p|^2), \quad (8)$$

where  $N$  is a normalization constant, and  $\ell_i = m_i + n_i$  is the z-projection of the angular momentum of the basis function. The exponents  $\alpha_i$  were optimized for a single Gaussian well and a single atom separately, and supplemented with extra functions when used together. For our calculations a basis set of  $2s2p$  functions for the dots, and  $5s5p1d1f$  for the atom was found to achieve converged results for the energy spectrum.

The numerical results presented in this work refers to those corresponding to the parameters of GaAs: effective mass  $m^* = 0.067m_e$ , effective dielectric constant  $\epsilon = 13.1$ , Bohr radius  $a_B^* = 10$  nm and effective atomic unit of energy  $1 \text{ Hartree}^* = 10.6 \text{ meV}$  [42,48].

The depth of the Gaussian potentials modelling the dots are taken as  $V_0 = 4 \text{ Hartree}^* = 42.4 \text{ meV}$ , and its typical range  $a = \sqrt{2} a_B^* = 14.1 \text{ nm}$ , with an interdot separation  $22.5 \text{ nm}$ . Smaller interdot separations provides a high electric dipole moment and, hence, strong coupling with the external field but induce delocalization of the electrons making difficult to define the occupation on a single dot. Larger interdot separation produces the opposite effect, with the drawback of small coupling with the laser electric field, thus worsening the controllability of the QDs.

## 2.2. Optimal control theory for electrons interacting with a time-dependent electric field

Let us consider a time-dependent electric field  $\boldsymbol{\varepsilon}(t)$  pointing along the line joining the QDs ( $x$  direction) and propagating along the  $z$  direction (perpendicular to the plane of the system). The time evolution of the electron state, assuming the dipole approximation for the interaction, will be given by

$$i \frac{\partial \Psi(t)}{\partial t} = H \Psi(t) \quad (9)$$

$$H = H_0 - \mu \varepsilon(t) \quad (10)$$

where  $\mu$  is  $x$ -component of the dipole moment operator.

Application of optimal control theory (OCT) allows to design a pulse of duration  $T$ , whose interaction drives the system to a state  $\Psi(T)$ , having maximum overlap to a given state  $\phi_F$  or, equivalently, maximizes the expectation value of the operator  $\mathcal{O} = |\phi_F\rangle\langle\phi_F|$  at the end of the pulse application [25]:

$$J_1[\Psi] = |\langle\Psi(T)|\phi_F\rangle|^2 \quad (11)$$

where  $J_1$  is known as the yield. In order to avoid high energy fields we introduce a second functional

$$J_2[\boldsymbol{\varepsilon}] = -\alpha \left[ \frac{1}{T} \int_0^T \boldsymbol{\varepsilon}^2(t) dt - F \right] \quad (12)$$

where the time-integrated intensity is known as the fluence of the field,  $F$  is the fixed fluence and  $\alpha$  is a time-independent Lagrange multiplier. In addition the electronic wave function has to satisfy the time-dependent Schrödinger equation, introducing a third functional:

$$J_3[\boldsymbol{\varepsilon}, \Psi, \chi] = -2 \text{Im} \int_0^T \left\langle \chi(t) \left| \frac{\partial}{\partial t} - H(t) \right| \Psi(t) \right\rangle \quad (13)$$

where we have introduced the time-dependent Lagrange multiplier  $\chi(t)$ . Finally, the Lagrange functional has the form  $J = J_1 + J_2 + J_3$ . The Variation of this functional with respect to  $\Psi(t)$ ,  $\boldsymbol{\varepsilon}(t)$  and  $\chi(t)$  allows us to obtain the control equations [30]

$$i \frac{\partial \Psi(t)}{\partial t} = H \Psi(t), \quad \Psi(t=0) = \phi(\mathbf{r}_1, \mathbf{r}_2) \quad (14)$$

$$\frac{\partial \chi(t)}{\partial t} = H(t) \chi(t), \quad \chi(T) = |\phi_F\rangle\langle\phi_F| \Psi(T) \quad (15)$$

$$\boldsymbol{\varepsilon}(t) = -\frac{1}{\alpha} \text{Im} \langle \chi(t) | \hat{\mu} | \Psi(t) \rangle \quad (16)$$

$$\int_0^T \boldsymbol{\varepsilon}^2(t) dt = A_0 \quad (17)$$

This set of coupled equations can be solved iteratively, for example, using the efficient forward-backward propagation scheme developed in [31]. The algorithm starts by propagating  $\phi(\mathbf{r}_1, \mathbf{r}_2)$  forward in time, using in the first step a guess of the electric field  $\boldsymbol{\varepsilon}^0(t)$ . At the end of this step we obtain the wave function  $\Psi^{(0)}(\mathbf{r}_1, \mathbf{r}_2, T)$ , which is used to evaluate  $\chi^{(0)}(\mathbf{r}_1, \mathbf{r}_2, T) = |\phi_F\rangle\langle\phi_F| \Psi^{(0)}(\mathbf{r}_1, \mathbf{r}_2, T)$ . The algorithm continues with propagating  $\chi^{(0)}(\mathbf{r}_1, \mathbf{r}_2, t)$  backwards in time. In this step we need to know both wave functions ( $\Psi^{(0)}$  and  $\chi^{(0)}$ ) at the same time. In this step we obtain the first optimized pulse  $\boldsymbol{\varepsilon}^1(t)$ . We repeat this operation until the convergence of  $J$  is achieved. The Lagrange multiplier  $\alpha$  is calculated using the fixed fluence following the calculation details showed in reference [31]. The numerical integration of the forward and backward time evolution was performed using fourth-order Runge-Kutta algorithms.

As usual in this technique, we constrain the field using an envelope function [26,30],

$$f(t) = \frac{1}{2} \left\{ \text{erf} \left[ \frac{a}{T} \left( t - \frac{T}{b} \right) \right] + \text{erf} \left[ \frac{-a}{T} \left( t - T + \frac{T}{b} \right) \right] \right\} \quad (18)$$

in order to have a electromagnetic pulse  $\boldsymbol{\varepsilon}(t)$  with a finite duration, i.e.,  $\boldsymbol{\varepsilon}(0) = \boldsymbol{\varepsilon}(T) = 0$ . Furthermore, a spectral cut-off is applied to remove frequency components higher than a prescribed threshold  $\omega_c$  [31].

## 3. Controllability of the charge qubit states in the presence of an impurity

Firstly, we will analyze the controllability of a symmetrical DQD in a clean sample. The absence of impurities means that the only relevant potentials are those from the confining wells. Then, the electronic ground state,  $\Psi_0(\mathbf{r}_1, \mathbf{r}_2)$ , is spatially delocalized, with a high density around each dot. The first and second excited states,  $\Psi_1$  and  $\Psi_2$ , have very close energies, what allows one to define the doubly occupied states at the left and right dots as  $\Psi_{LL/RR}(\mathbf{r}_1, \mathbf{r}_2) = 2^{-1/2} [\Psi_1(\mathbf{r}_1, \mathbf{r}_2) \pm \Psi_2(\mathbf{r}_1, \mathbf{r}_2)]$ . Let us consider one of them, say  $\Psi_{RR}$ , as the target state for optimizing the electric pulse. Thus the optimal field will produce a delocalization-localization transition of the electron charge, which could be detected by measuring the charge variation at the dots. Fig. 1 shows the yield obtained in the transition  $\Psi_0 \rightarrow \Psi_{RR}$  where one electron is moved from the left to the right dot. As we can observe in the lower panel of Fig. 1, for a fixed fluence, a high yield is obtained by extending the pulse duration. On the other hand, for a given duration of the pulse, the yield becomes larger as the fluence increases (as shown in upper panel of Fig. 1). Therefore, the most convenient situation corresponds to that where a long pulse of high intensity is applied. However, the pulse duration cannot be arbitrarily long because the coherence time have the order of nanoseconds. So, in order to perform operations cyclically with the qubit, the pulse has to be restricted to tens or hundreds of picoseconds.

Now consider the effect produced by charged impurities. If the sample were heavily doped, that is, it has a high impurity density or their charges are high (i.e., comparable to the electron charge) the system is far from being controllable. Therefore, we shall consider the situation where the density of impurities is low, such that no more than one of them is in the neighbourhood of the DQD. We also assume that their charge  $Ze$  is small, characterized by an effective parameter  $Z < 0.5$

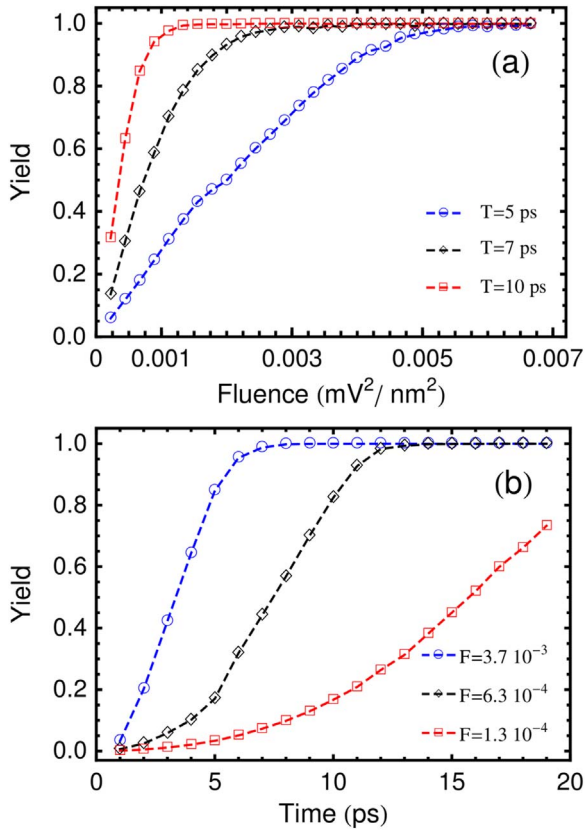


**Fig. 1.** (a) Yield as a function of fluence  $F$ , for three different values of pulse duration  $T=5, 7$  and  $10$  ps. (b) Yield as a function of time duration of the pulse for three different values of fluence,  $F = 3.7 \times 10^{-3}, 6.3 \times 10^{-4}$  and  $1.3 \times 10^{-4} \text{ mV}^2/\text{nm}^2$  ps.

(meaning that it is highly screened), a range which has been considered suitable in a previous work [65].

Fig. 2 shows the calculated yield obtained when the pulse optimized for the transition  $\Psi_0 \rightarrow \Psi_{RR}$  in the clean DQD, is applied to the doped DQD having a Coulomb point charge  $Ze$  located at the mid point between both quantum dots. Fig. 2 shows that for ultrashort pulses of a few picoseconds, even very small impurity charges can heavily deteriorate the performance of the optimal pulse. The unintentional impurities act as trapping centers for the electrons, spoiling the fast operation of the pulses optimally designed for the clean device.

In the next section we propose and discuss a protocol for controlling the electronic states using OCT in order to avoid the deterioration introduced by a charge impurity located in between the dots.

#### 4. OCT-based two-step protocol

Although the OCT pulses produce fast transitions between localized and delocalized states in a clean DQD, with high fidelity, they fail after adding a Coulomb charge. This is due to the fact that, in the presence of the charge, the spatial distribution of the electron wave function of the system is not only localized around the QDs, but also in the proximity of the center of the Coulomb potential. Nevertheless, for a proper operation and detection of the electron charges in the QDs (e.g., using quantum point contacts) it is desirable that both the initial and target qubit states correspond to electron densities predominantly localized around the QDs.

Our proposed protocol consists in using OCT for tailoring two pulses, to be sequentially applied, in order to induce the transitions  $\Psi_0 \rightarrow \Psi_0^{(0)} \rightarrow \Psi_{RR}^{(0)}$ . Firstly, an *initialization* pulse is designed for the transition  $\Psi_0 \rightarrow \Psi_0^{(0)}$ , i.e., a pulse by which the electrons initially in the ground state of the Hamiltonian with the impurity ( $H^{(Z)}$ ) are set in the ground state of the Hamiltonian without impurity ( $H^{(0)}$ ). Immediately

afterwards, the second pulse drives the wave function to perform the same transition as in the clean system, i.e.,  $\Psi_0^{(0)} \rightarrow \Psi_{RR}^{(0)}$ . This second pulse has all the previously discussed advantages of fast and high-fidelity evolution, and correspond to the desired *qubit operation*, e.g., for information processing.

The influence of the impurity charge could, in principle, spoil and slow down the whole process because it enters in two ways: (i) the initialization pulse introduces an additional evolution time to set the wave function in the state  $\Psi_0^{(0)}$ . As a consequence, the operation of the device with an impurity, performed between the same pair of states, will be necessarily slower than without impurities present, and the fidelity, for a fixed pulse duration, could depend strongly on  $Z$ ; (ii) although the operation pulse produces a transition between impurity-free states  $\Psi_0^{(0)}$  and  $\Psi_{RR}^{(0)}$ , they are to be represented in terms of states of the whole Hamiltonian as  $\Psi_i^{(0)} = \sum_j c_{ij}(Z) \Psi_j$ , with coefficients depending on the charge  $Z$ . We shall show in the following, however, that none of these circumstances eliminates the advantages of the procedure, which holds a high fidelity with operation times lesser than the typical dephasing times.

##### 4.1. Initialization of the qubit

We consider three different values for the charge of the impurity, namely,  $Z=0.1, 0.2$  and  $0.3$ , corresponding to the conditions of weak and intermediate strength of the Coulomb potential competing with the confining ones in the QDs.

Firstly, we calculated pulses by optimizing them without imposing any restriction on the maximum allowed frequency. As a result, the yield increases monotonically with the fluence until reaching a plateau having a maximum value of 99.9% for  $Z=0.1\%$  and 99.4% for  $Z=0.3$ . These maximum yields are reached nearly at  $F = 1.3 \times 10^{-3} \text{ mV}^2/\text{nm}^2$ . On the other hand, when a cut-off frequency  $\omega_c$  is imposed, the increase in the yield is similar until the aforementioned value of fluence. Nevertheless, instead of the plateaus of the unconstrained pulses, the yield of frequency-constrained pulses reaches a top and then oscillates, with a slight decrease in average. Remarkably, the use of a cut-off frequency  $\omega_c = 20$  THz, compatible with current experimental capabilities, affects more strongly the yield of the systems with smaller impurity charges. This behaviour can be attributed to the fact that, for low fluence pulses, the electron can only be promoted to the low-lying levels having small excitation energy. On the other hand, pulses of larger fluence entail a larger amplitude and excitation energies to higher states. While the unconstrained pulses have a suitable frequency composition to produce the excitation to the higher levels, the frequency constrained pulses do not have the higher

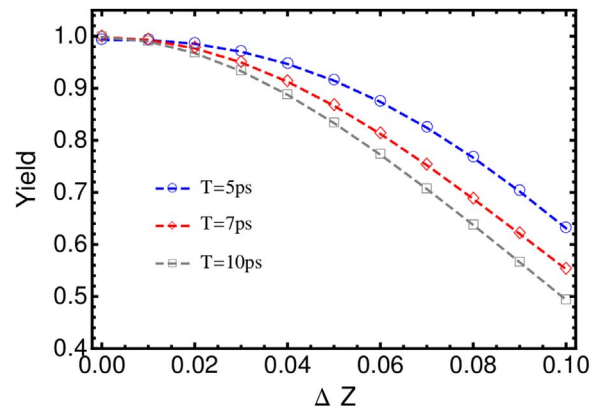


**Fig. 2.** Calculated yields for pulses of 5, 7 and 10 ps as a function of the magnitude of the effective charge  $Z$  of an impurity localized in the middle of the dots. The pulses were optimized for the double quantum dot without impurity, with a fluence of  $F = 1.3 \times 10^{-3} \text{ mV}^2/\text{nm}^2$ , and applied to the system containing the Coulomb impurity. The yield is nearly 1 for  $Z=0$ , but it becomes strongly deteriorated even for small values of  $Z$ .



frequency required to excite the electrons to the higher levels. Therefore, some transitions involving highly excited states are inhibited, leading to a decrease in the yield. In other words, for systems with a large impurity charge, its electronic structure is mainly determined by the lowest lying (i.e., by the low frequency or low excitation energy) states of the Coulomb potential. Therefore, in such cases, both pulses, with and without cut-off, are almost equally well suited for producing the maximum yield which, nevertheless, becomes smaller than for small impurity charges.

We assessed the approach to the target state along the time by designing a 10 ps pulse having a cut-off frequency  $\omega_{\max} = 20$  THz for three values of  $Z$  (Fig. 3). Fig. 3 shows the result of applying OCT to initialize the DQD device. The yield reaches a high value after about  $10^3$  iterations of the optimization procedure, although typically  $10^4$  iterations have been used in the calculations. The Fourier spectrum of the optimized pulses show only a few relevant frequencies giving smoothly oscillating fields experimentally realizable. These initialization pulses have different characteristics depending on the magnitude of the impurity charge. For the system with  $Z=0.1$ , the electron population of the ground state is gradually transferred to the first excited state until approximately a half of the pulse length, when both occupations reach about 70% and 30%, respectively. In the second half of the pulse, the electron population is again restored to the ground state. Only the two lowest states are involved in the transition  $\Psi_0 \rightarrow \Psi_0^{(0)}$  because, for small  $Z$ , both ground states are rather similar, and the pulse frequency is mainly determined by the energy difference between the ground and first excited states of  $H^{(Z)}$ .

Fig. 4 shows the form of the optimized 10 ps pulse (upper panel) and the time dependence of the level occupations for the low lying states for  $Z=0.3$  resulting from its application (lower panel). The pulse, although quite simple, is not monochromatic; the most relevant frequencies in its spectral composition are shifted downwards due to the level mixing between the DQD and the charged Coulomb ion, which have a smaller energy separation. The three dominant frequencies  $\omega_{ij}$  can be identified as related to transitions between the low-lying levels  $\Psi_i \rightarrow \Psi_j$ , with the main contribution coming from  $\omega_{01} \approx 14$  THz and minor ones from  $\omega_{12} \approx 0.13$  THz and  $\omega_{24} \approx 4.6$  THz. The lower panel of Fig. 4 shows the time variation of the level occupation for the first five states during application of the pulse. The ground state occupation  $n_0$  decreases less than 10% by the mid of the pulse duration, transferring population to the first excited state and, to less extent, to the second and fourth excited states. At the end of the pulse, the population  $n_0$  remains high (close to 95%) while the rest populates the state  $\Psi_3^Z$  and  $\Psi_2^Z$ . In a wide range of cases studied, the pulses obtained from the OCT procedure for initialization of the qubit, under conditions of low fluence and frequency cut-off compatible with current experimental capabilities, have been found to be rather simple, fast and with fidelities higher than 99.9%.

#### 4.2. Operation of the qubit

We address now the problem of producing the transition of interest for operating the qubit,  $\Psi_0^{(0)} \rightarrow \Psi_{RR}^{(0)}$ , and how it is affected by the presence of the Coulomb charge. Fig. 5 shows the yield for the transition from the state  $\Psi_0^{(0)}$ , obtained with the initialization pulse discussed above, for  $Z=0.1, 0.2$  and  $0.3$ , together with the  $Z=0.0$  case for the sake of comparison. The pulses were optimized to induce fast transitions (10 ps duration), yet they still hold high fidelity with the desired target state. Interestingly, Fig. 5 shows that the system, in presence of the charge, evolves to the target state faster than the clean QDs. A yield of 90% can be reached in around 7 ps for the  $Z=0.3$  DQD, which is 2 ps shorter than for the clean system.

The optimal pulse for targeting the localized state  $\Psi_{RR}^{(0)}$ , after the initialization pulse, is shown at the upper panel in Fig. 6. The resulting yield and the variations of the occupation of the lower-lying states is depicted in the lower panel of Fig. 6. As shown, the transition mainly

involves the three lowest states of the DQD, namely, the ground state  $\Psi_0$ , and first and second excited states,  $\Psi_1$  and  $\Psi_2$ . The third and fourth excited states  $\Psi_3$  and  $\Psi_4$  also gives, to a less extent, some smaller contribution during the second half of the pulse. The yield reaches a value  $\geq 99.9\%$  after 10 ps, with a steadily increasing behaviour although with oscillations of  $\sim 10\%$  during the second half of the pulse (i.e., between 5 and 10 ps). The examination of the time dependence of the state occupations allows us to explain how the target state is built and this high fidelity is reached. During the firsts 4 ps, the population of the ground state is transferred almost exclusively to the state  $|1\rangle$ . In the next 4 ps (from 4 to 8 ps.) the population of the ground state  $|0\rangle$  continues decreasing monotonically but part of the electronic charge is also transferred to the state  $|2\rangle$ . As a remarkable feature of the figure, the occupations of the states  $|1\rangle$  and  $|2\rangle$  show complementary peaks and dips of oscillations mounted on a smooth variation. Peaks of one curve occurs at the dips of the other, entailing that part of the charge is oscillating between states  $|1\rangle \leftrightarrow |2\rangle$ . Finally, during the last 2 ps. the states  $|1\rangle$  and  $|2\rangle$  approach to be nearly equally populated in order to reach the target state. Nevertheless, there is a small but observable difference between them due to the occupation of higher excited states.

The dynamical process of reaching the target state described above, and the influence of the impurity charge on the controllability, can be understood from an analysis of the electronic structure of our system, as sketched in Fig. 7. It shows the two electron wave function along the  $x$  axis joining both dots,  $\Psi_i(x_1, 0; x_2, 0)$ , as a contour plot of the variables  $(x_1, x_2)$ , for the three lowest energy levels of the DQD without impurities (Fig. 7a) and in the presence of an impurity of charge  $Z=0.3$  (Fig. 7b). Positive and negative  $x_i$  coordinates refer to positions of electron  $i$  close to right and left wells, respectively. When the two-electron state corresponds to a situation where, spatially, each electron is in a different well, the wave function have large values along the  $x_1 = -x_2$  diagonal ( $\searrow$ ) and represents a delocalized two-electron state. On the other hand, high values around the diagonal  $x_1 = x_2$  ( $\nearrow$ ) entails for double occupation, i.e., when both electrons are in one of the wells. Therefore, irrespective of the presence or not of the Coulomb charge, Figs. 7a and 7b show that the ground state  $|0\rangle$  is a two-electron state describing electrons delocalized at different wells. Excited states  $|1\rangle$  and  $|2\rangle$ , on the other hand, are mainly along the  $\nearrow$  direction, i.e., they represent double occupation of the wells. State  $|1\rangle$  has a nodal line along direction  $\searrow$  while  $|2\rangle$  has not, meaning that  $|1\rangle$  and  $|2\rangle$  have ungerade and gerade symmetry under inversion through the interdot center  $x=0$ . The changes in the states from Fig. 7a to Fig. 7b, due to the charge  $Z$ , are apparent; states with  $Z \neq 0$  have a noticeable contribution from the impurity location  $x_1 = x_2 = 0$ . More information, to be discussed below, is provided in panels (c) and (d); they show the

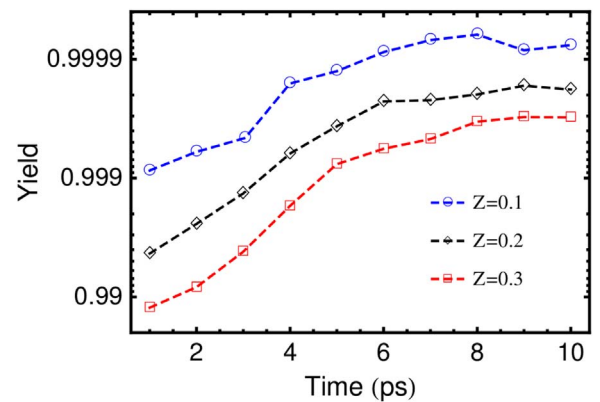
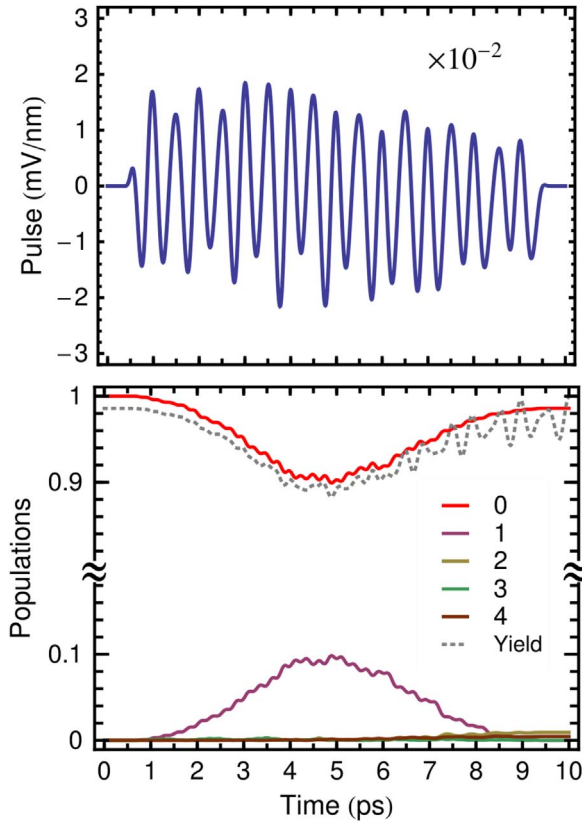
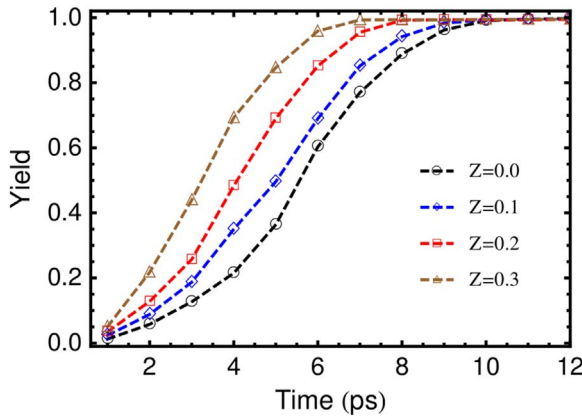


Fig. 3. Yield of the initialization pulse of fluence  $F = 1.3 \times 10^{-4} \text{ mV}^2/\text{nm}^2$  as a function of time for the double quantum dot with a Coulomb charge  $Z$  placed in the middle of the segment of line joining the centers of the dots. Application of this pulse prepares the system to be used as a qubit, evolving the actual ground state of the system with an impurity,  $\Psi_0$ , to the ground state of the system having no impurity,  $\Psi_0^{(0)}$ .



**Fig. 4.** Upper panel: pulse of the initialization as a function of time for  $F = 1.3 \times 10^{-4} \text{ mV/nm}^2$  for the double quantum dot with a Coulomb charge  $Z=0.3$  placed in the middle of the segment of line joining the centers of the dots. Application of this pulse prepares the system to be used as a qubit, evolving the actual ground state of the system with an impurity  $\psi_1^{(Z=0.3)}$  to the ground state of the system having no impurity  $\psi_1^{(0)}$ . Lower panel: evolution of the different states as a function of time.



**Fig. 5.** Yield of the operation pulse of fluence  $F = 1.3 \times 10^{-3} \text{ mV}^2/\text{nm}^2$  as a function of time for the double quantum dot with a Coulomb charge  $Z$  (for  $Z=0.0$  (black circles),  $Z=0.1$  (blue squares),  $Z=0.2$  (red squares) and  $Z=0.3$  (brown triangles)) placed in the middle of the segment of line joining the centers of the dots. Application of this pulse produces the transition between the localized ground state of the DQD without Coulomb impurity and the state where both electrons are localized at the right dot. (For interpretation of the references to color in this figure legend, the reader is referred to the web version of this article.)

dependence of the electronic energy of the five lowest states (Fig. 7c) and the two matrix elements of the dipole operator  $X = x_1 + x_2$  that give rise to the most relevant transitions (Fig. 7d), as a function of the Coulomb charge  $Z$ , respectively.

Further insight can be gained by approximating the system by a two-sites Hubbard model having hopping  $w$ , on-site Coulomb repul-

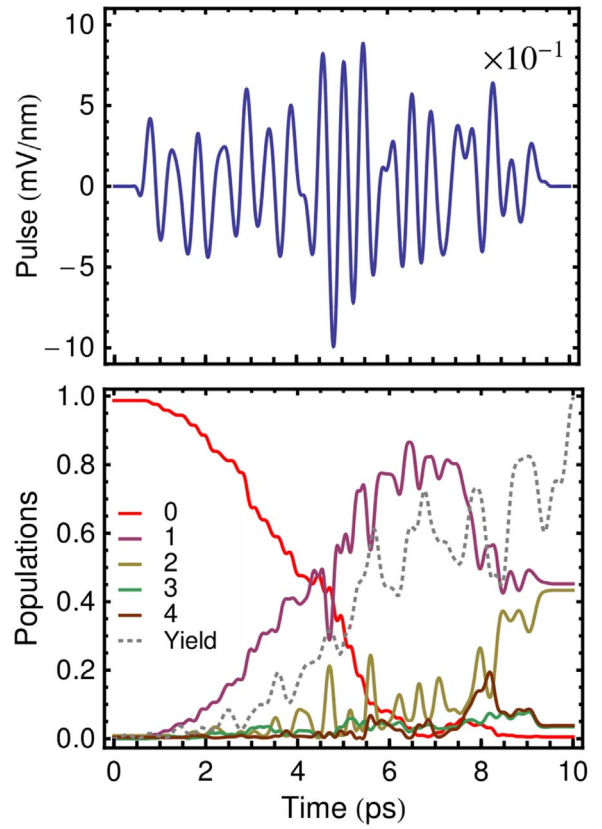


**Fig. 6.** Upper panel: pulse of the operation as a function of time for  $F = 1.3 \times 10^{-3} \text{ mV}^2/\text{nm}^2$  for the double quantum dot with a Coulomb charge  $Z=0.3$  placed in the middle of the segment of line joining the centers of the dots. Lower panel: evolution of the different states as a function of time.

sion  $U$ , and one orbital per site  $\varphi_A$  ( $A=L, R$ ). Assuming zero on-site energies for both wells and strong repulsion ( $w \ll U$ ), its three lowest (non-normalized) singlet states and energies are

$$\Psi_0 = \Psi_S^g + \mathcal{O}\left(\frac{w}{U}\right)\Psi_D^g, \quad E_0 \approx -\frac{4w^2}{U} \quad (19)$$

$$\Psi_1 = \Psi_D^u, \quad E_1 = U \quad (20)$$

$$\Psi_2 = \Psi_D^g + \mathcal{O}\left(\frac{w}{U}\right)\Psi_S^g, \quad E_2 \approx U + \frac{4w^2}{U} \quad (21)$$

The subscripts S and D stand for single or double occupation of the on-site orbitals  $\varphi_{L,R}$ , and the superscripts  $u$  and  $g$  refer to the inversion symmetry (gerade or ungerade) with respect to the interdot center. In the strongly correlated regime,  $E_1$  and  $E_2$  are quasi-degenerates, as in our CI calculations (Fig. 7c). In such regime, our target state can be approximated as  $\Psi_{RR} = (\Psi_D^g - \Psi_D^u)/2 \approx (\Psi_2 - \Psi_1)/2$ . Due to the point symmetry, dipole matrix elements  $\mu_{ij} = \langle \Psi_i | X | \Psi_j \rangle$  are such that  $\mu_{02} = 0$ , but  $\mu_{01} \neq 0 \neq \mu_{12}$ . Hence, transitions  $0 \leftrightarrow 1 \leftrightarrow 2$  are allowed, but  $0 \leftrightarrow 2$  is not, as it is actually the case in our CI calculations. Within this model,  $\mu_{01} = (4w/U)x_{LL}$  and  $\mu_{12} = 2x_{LL}$ , with  $x_{LL} = \int \varphi_L^2(\mathbf{r})x d\mathbf{r}$  being the matrix element calculated in terms of the orbital centered at the left well  $\varphi_L$ . Therefore, from this approximate model a relation  $\mu_{01}/\mu_{12} = 2w/U$  is expected, with a transition probability lower for  $0 \leftrightarrow 1$  than for  $1 \leftrightarrow 2$ . The corresponding resonant frequencies are in the relation  $\omega_{12}/\omega_{01} \approx 4w^2/U^2 \ll 1$ . The dynamics of our system can be thought in terms of this three-levels Hubbard model as follows: starting from the ground state  $|0\rangle$  [Eq. (19)], the external electric field induces transitions  $0 \leftrightarrow 1$  increasing the occupation of the first excited state, while  $|2\rangle$  remains empty because  $0 \leftrightarrow 2$  is forbidden. After some time, part of the population of  $|1\rangle$  is transferred to  $|2\rangle$  due to the large  $\mu_{12}$ . These processes need to be excited with frequencies  $\omega_{01}$  and  $\omega_{12}$ . The

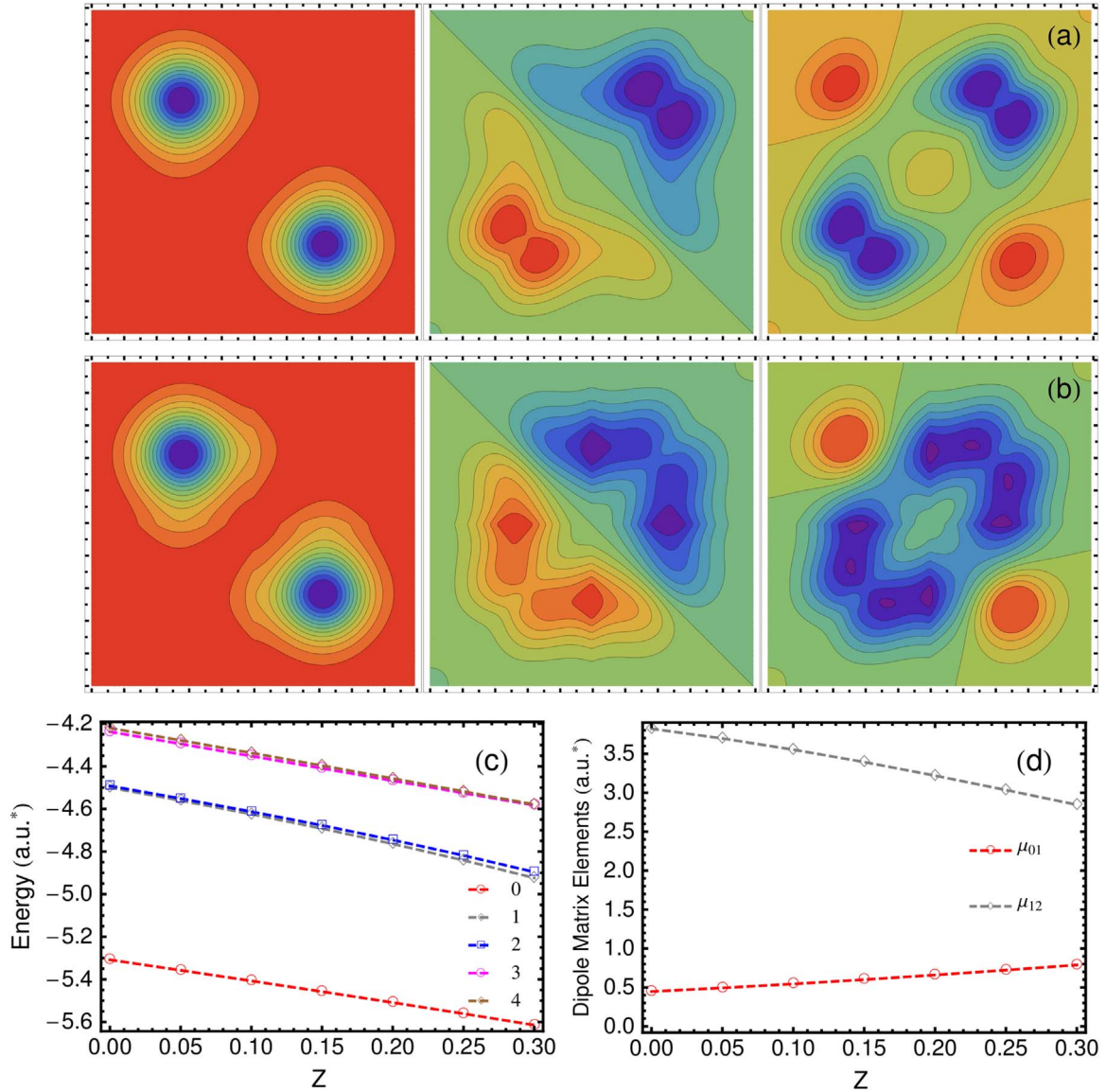


**Fig. 7.** The calculated electronic structure of the double quantum dot. (a)-(b): Contour plot picture of the ground and two first excited states wave functions along the interdot line of the DQD without (a) and with (b) a Coulomb impurity charge  $Z=0.3$  as a function of the  $x_1$  and  $x_2$  electron coordinates. Approximate expressions of the states are given by Eqs. (19)–(21). (c) Variation of the low-lying electronic energies as a function of the charge  $Z$ , (d) Variation of the dipole moments  $\mu_{01}$  and  $\mu_{12}$  as a function of  $Z$ .

spectral composition of our optimally designed pulse of length  $T$  shows two important contributions: one at  $\omega_{01} \approx 14$  THz and other at a low frequency, which cannot be resolved because is less than  $2\pi/T$ , but could be related to  $\omega_{12}$ . Since our target state  $|RR\rangle$  requires to populate both  $|1\rangle$  and  $|2\rangle$ , the processes continues until both become evenly populated. The presence, in our CI calculations, of the state  $|4\rangle$  and higher levels (not included in the approximate model) having a non vanishing dipole moment matrix element  $\mu_{24}$ , produce some leakage, giving rise to the population of  $|4\rangle$  observed in our calculations (Fig. 6).

To some extent, the effect of the low charge impurities can also be understood from the approximate Hubbard model. It can be shown that the effect of the addition of a one-electron operator to the Hubbard Hamiltonian is accounted for by a change in the hopping parameter  $w \rightarrow w' = w + \delta w$ , with  $\delta w \sim -Z$  for the Coulomb charge one-electron operator. The dipole moment operator  $X = x_1 + x_2$  has matrix elements  $\langle \Psi_3^0 | X | \Psi_0^0 \rangle = 0$  but  $\langle \Psi_2^0 | X | \Psi_0^0 \rangle \neq 0$ . The relative contribution of  $|\Psi_2^0\rangle$  increases with  $w$  (and therefore with  $Z$ ) in  $|0\rangle$  but decreases in  $|2\rangle$  [Eqs. (19) and (21)] while  $|1\rangle$  is independent of  $w$ . Hence  $\mu_{01}$  increases, while  $\mu_{12}$  decreases, linearly with the impurity charge  $Z$ . The energy differences  $\hbar\omega_{01}$  and  $\hbar\omega_{12}$  do not change (at first order in  $Z$ ) because

all three energy eigenvalues share the same dependence. In our CI calculations, the probability of dipole transitions  $0 \leftrightarrow 1$  increases at a lower rate than the decreasing of the one for transitions  $1 \leftrightarrow 2$  (Fig. 6d). As a consequence, if the pulse designed for the DQD without impurity, containing frequencies  $\omega_{01}$  and  $\omega_{12}$ , is applied to the system doped with a charged impurity, the whole processes is slower and, at the end of the pulse duration, the resulting final state have a lower fidelity.

In spite of the usefulness of the approximate Hubbard model for interpreting the results, one should be warned that the detailed electronic structure of the DQD becomes more and more relevant as higher values of fluence of the field are considered because of the increasing influence of the higher energy levels.

The complete pulse resulting from the application of the proposed protocol and the time evolution of the level occupation of the system with  $Z=0.3$  is depicted in Fig. 8. The vertical line at  $t=8$  ps separates the two steps of the process, i.e., 8 ps. for initialization and, then, 10 ps for operation of the qubit. Although in a device running tasks for information processing, the qubit transition will have to be run many times, the initialization step would be required just once; thus the whole process is not strongly affected by the impurity.



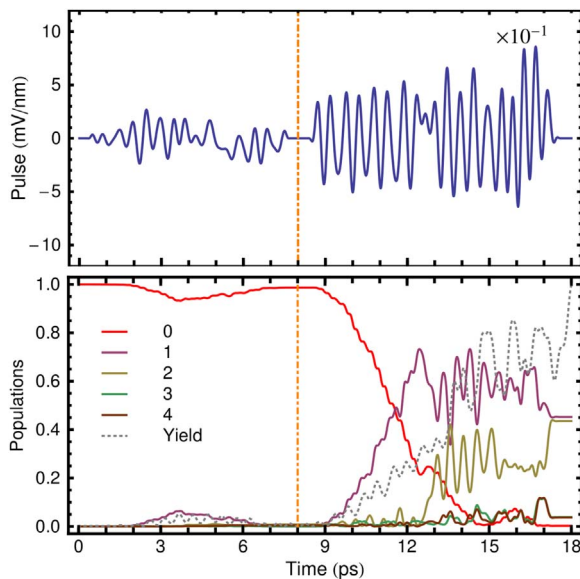


**Fig. 8.** Initialization and operation of the charge qubit in a double quantum dot with a Coulomb impurity. The fluence of the pulse in the initialization step is  $F = 1.3 \times 10^{-4} \text{ mV}^2/\text{nm}^2$  whereas in the operation step it is of one higher order. Upper panel: Complete pulse designed in order to initialize and operate the doped device ( $Z=0.3$ ). Lower panel: Population of the five lowest energy states during the transition  $\psi_0 \rightarrow \psi_0^{(0)} \rightarrow \psi_{RR}^{(0)}$ .

## 5. Conclusions

We have studied the efficiency of OCT based pulses suitable to produce transitions between localized and delocalized states of a double quantum dot device, with or without unintentional impurities. Those transitions give rise to changes of the electron charge in the individual dots, which can be detected, thus experimentally realizing a charge qubit. The resulting fast and high-fidelity tailored pulses are able to operate the qubit in times of the order of 10 ps, shorter than the decoherence time in clean samples, but their fidelity deteriorates heavily when even small Coulomb charges are present in the system. Therefore, we proposed and assessed the performance of applying a two-step protocol, by firstly initializing the electronic states in the ground state of the system without impurities, such that it compensates the changes in the electronic structure suffered by the DQD, introduced by the Coulomb charge. The second pulse operates the qubit as if it were impurity-free. Since both steps are designed in terms of the real electronic structure of the charged qubit, we have also analyzed the influence of the charge  $Z$  on the electronic states of the double quantum dots. We have found that the complete two-step protocol involves mainly the lowest lying energy levels and remains fast enough to drive the states to the desired target state with a high fidelity, compatible with the requirements for its use in information processing tasks.

## Acknowledgements

We would like to acknowledge CONICET (PIP 112-201101-00981), SGCyT(UNNE) and FONCyT (PICT-2012-2866) for partial financial support of this project.

## References

[1] D. Loss, D.P. DiVincenzo, *Phys. Rev. A* 57 (1998) 120.  
 [2] D.P. DiVincenzo, *Science* 309 (2005) 2173.  
 [3] J.R. Petta, A.C. Johnson, J.M. Taylor, E.A. Laird, A. Yacoby, M.D. Lukin, C.M. Marcus, M.P. Hanson, A.C. Gossard, *Science* 309 (2005) 2180.  
 [4] R. Brunner, Y.S. Shin, T. Obata, M. Piore-Ladrière, T. Kubo, K. Yoshida,

T. Taniyama, Y. Tokura, S. Tarucha, *Phys. Rev. Lett.* 107 (2011) 146801.  
 [5] W.G. van der Wiel, S. De Franceschi, J.M. Elzerman, T. Fujisawa, S. Tarucha, L.P. Kouwenhoven, *Rev. Mod. Phys.* 75 (2003) 1.  
 [6] R. Hanson, L.P. Kouwenhoven, J.R. Petta, S. Tarucha, L.M.K. Vandersypen, *Rev. Mod. Phys.* 79 (2007) 1217.  
 [7] S.J. Lee, S. Souma, G. Ihm, K.J. Chang, *Phys. Rep.* 394 (2004) 1.  
 [8] W. Pötz, W.A. Schroeder, (Eds.), *Coherent control in atoms, molecules, and semiconductors*, (Kluwer Academic, Dordrecht), 1999.  
 [9] M.O. Scully, M.S. Zubairy, *Quantum Optics*, Cambridge University Press, Cambridge, UK, 1997.  
 [10] H. Rabitz, R. de Vivie-Riedle, M. Motzkus, K. Kompka, *Science* 288 (2000) 824.  
 [11] G. Murgida, D.A. Wisniacki, P. Tamborenea, *Phys. Rev. Lett.* 99 (2007) 036806.  
 [12] A. Ferrón, O. Osenda, P. Serra, *J. Appl. Phys.* 113 (2013) 134304.  
 [13] D.S. Acosta Coden, R.H. Romero, E. Räsänen, *J. Phys.: Cond. Matter* 27 (2015) 115303.  
 [14] E. Räsänen, A. Castro, J. Werschnik, A. Rubio, E.K.U. Gross, *Phys. Rev. Lett.* 98 (2007) 157404.  
 [15] E. Räsänen, A. Castro, J. Werschnik, A. Rubio, E.K.U. Gross, *Phys. Rev. B* 77 (2008) 085324.  
 [16] T. Hayashi, T. Fujisawa, H.D. Cheong, Y.H. Jeong, Y. Hirayama, *Phys. Rev. Lett.* 91 (2003) 226804.  
 [17] J.R. Petta, A.C. Johnson, C.M. Marcus, M.P. Hanson, A.C. Gossard, *Phys. Rev. Lett.* 93 (2004) 186802.  
 [18] J.Q. Zhang, S. Vitkalov, Z.D. Kvon, J.C. Portal, A. Wieck, *Phys. Rev. Lett.* 97 (2006) 226807.  
 [19] W.S. Warren, H. Rabitz, M. Dahleh, *Science* 259 (1993) 1581.  
 [20] A.M. Weiner, D.E. Leaird, J.S. Patel, J.R. Wullert, *IEEE J. Quantum Electron.* 28 (1992) 908.  
 [21] A. Assion, T. Baumert, M. Bergt, T. Brixner, B. Kiefer, V. Seyfried, M. Strehle, G. Gerber, *Science* 282 (1998) 919.  
 [22] L. Polachek, D. Oron, Y. Silberberg, *Opt. Lett.* 31 (2006) 5.  
 [23] M. Plewicky, S.M. Weber, F. Weise, A. Lindinger, *Appl. Phys. B* 86 (2006) 259.  
 [24] M. Plewicky, F. Weise, S.M. Weber, A. Lindinger, *Appl. Opt.* 45 (2006) 8354.  
 [25] J. Werschnik, E.K.U. Gross, *J. Phys. B* 40 (2007) R175.  
 [26] K. Sundermann, R. de Vivie-Riedle, *J. Chem. Phys.* 110 (1999) 1896.  
 [27] W. Zhu, J. Botina, H. Rabitz, *J. Chem. Phys.* 108 (1998) 1953.  
 [28] Y. Maday, G. Turinici, *J. Chem. Phys.* 118 (2003) 8191.  
 [29] Y. Ohtsuki, G. Turinici, H. Rabitz, *J. Chem. Phys.* 120 (2004) 5509.  
 [30] A. Putaj, E. Räsänen, *Phys. Rev. B* 82 (2010) 165336.  
 [31] R. Kosloff, S. Rice, P. Gaspard, S. Tersigni, D. Tannor, *Chem. Phys.* 139 (1989) 201.  
 [32] W. Zhu, H. Rabitz, *J. Chem. Phys.* 109 (1998) 385.  
 [33] D. Sugny, C. Kontz, M. Ndong, Y. Justum, G. Dive, M. Desouter-Lecomte, *Phys. Rev. A* 74 (2006) 043419.  
 [34] D. Sugny, M. Ndong, D. Lauvergnet, Y. Justum, M. Desouter-Lecomte, *J. Photochem. Photobiol. A* 190 (2007) 359.  
 [35] D. Loss, D.P. DiVincenzo, *Phys. Rev. A* 57 (1998) 120.  
 [36] L. Saelen, R. Nepstad, I. Degani, J.P. Hansen, *Phys. Rev. Lett.* 100 (2008) 046805.  
 [37] X. Hu, S. Das Sarma, *Phys. Rev. A* 61 (2000) 062301.  
 [38] J. Werschnik, E.K.U. Gross, *J. Opt. B* 7 (2005) S300.  
 [39] J. Werschnik, E.K.U. Gross, *J. Phys. B* 40 (2007) R175.  
 [40] E. Räsänen, T. Blasi, M.F. Borunda, E.J. Heller, *Phys. Rev. B* 86 (2012) 205308.  
 [41] E. Räsänen, E.J. Heller, *Eur. Phys. J. B* 86 (2013) 17.  
 [42] T.T. Nguyen Nga, S. Das Sarma, *Phys. Rev. B* 83 (2011) 235322.  
 [43] D.S. Acosta Coden, R.H. Romero, A. Ferrón, S.S. Gomez, *J. Phys. B* 46 (2013) 065501.  
 [44] G. Bastard, *Phys. Rev. B* 24 (1981) 4714.  
 [45] R.C. Ashoori, H.L. Stormer, J.S. Weiner, L.N. Pfeiffer, S.J. Pearton, K.W. Baldwin, K.W. West, *Phys. Rev. Lett.* 68 (1992) 3088.  
 [46] Y. Wan, G. Ortiz, P. Phillips, *Phys. Rev. B* 55 (1997) 5313.  
 [47] E. Lee, A. Puzder, M.Y. Chou, T. Uzer, D. Farrelly, *Phys. Rev. B* 57 (1998) 12281.  
 [48] E. Räsänen, J. Könemann, R.J. Haug, M.J. Puska, R.M. Nieminen, *Phys. Rev. B* 70 (2004) 115308.  
 [49] P.A. Sundqvist, V. Narayan, S. Stafström, M. Willander, *Phys. Rev. B* 67 (2003) 165330.  
 [50] V. Nistor, L.C. Nistor, M. Stefan, C.D. Mateescu, R. Birjega, N. Solovieva, M. Nikl, *Superlattices Microstruct.* 46 (2009) 306.  
 [51] S.V. Nistor, M. Stefan, L.C. Nistor, E. Goovaerts, G. Van Tendeloo, *Phys. Rev. B* 81 (2010) 035336.  
 [52] V. Narayan, M. Willander, *Phys. Rev. B* 65 (2002) 125330.  
 [53] M. Schlosshauer, *Rev. Mod. Phys.* 76 (2005) 1267.  
 [54] C.H. Bennett, *Phys. Today* 48 (1995) 24.  
 [55] J. Xu, X. Xu, C. Li, C. Zhang, X. Zou, G. Guo, *Nat. Commun.* 1 (2010) 1.  
 [56] T. Yu, J.H. Eberly, *Phys. Rev. B* 66 (2002) 193306.  
 [57] A. Ferrón, D. Domínguez, M.J. Sánchez, *Phys. Rev. Lett.* 109 (2012) 237005.  
 [58] G.A. Álvarez, D. Suter, *Phys. Rev. Lett.* 104 (2010) 230403.  
 [59] A.P. Majtey, A.R. Plastino, *Int. J. Quantum Inf.* 10 (2012) 1250063.  
 [60] B. Bellomo, R. Lo Franco, G. Compagno, *Phys. Rev. Lett.* 99 (2007) 160502.  
 [61] T. Yu, J.H. Eberly, *Science* 323 (2009) 598.  
 [62] F. Lastra, S.A. Reyes, S. Wallentowitz, *J. Phys. B* 44 (2011) 015504.  
 [63] L. Viola, S. Lloyd, *Phys. Rev. A* 58 (1998) 2733.  
 [64] A.T. Kruppa, K. Arai, *Phys. Rev. A* 59 (1999) 3556.  
 [65] D.S. Acosta Coden, S.S. Gomez, R.H. Romero, *J. Phys. B* 44 (2011) 035003.  
 [66] S.S. Gomez, R.H. Romero, *Cent. Eur. J. Phys.* 7 (2009) 12.